Progress In Electromagnetics Research, Vol. 133, 535–554, 2013

A NEW METHOD FOR NON-LINE-OF-SIGHT VITAL SIGN MONITORING BASED ON DEVELOPED ADAPTIVE LINE ENHANCER USING LOW CENTRE FREQUENCY UWB RADAR

W. Z. Li, Z. Li, H. Lv, G. H. Lu, Y. Zhang, X. J. Jing, S. Li, and J. Q. Wang* †

College of Biomedical Engineering, The Fourth Military Medical University, Xi'an 710032, China

Abstract—The physiological parameters monitoring of human target are considered to be a meaningful and challenging task in non-line-of-sight (NLOS) scenes such as rescue of trapped survivors in post-disaster. In this paper, a new method based on developed adaptive line enhancer (DALE) is proposed to monitor vital signs via ultra-wideband (UWB) radar with centre frequency of 400 MHz. The validity of this new method is proved by means of two experiments with different positions of human target. The good results demonstrate that this new method can be used for vital sign monitoring including respiration and heartbeat through the obstacle. Furthermore, the motion responses due to respiration and heartbeat in different body positions are also discussed.

1. INTRODUCTION

The technology of non-contact vital sign detection has been used in bio-medical, surveillance, counterterrorism and rescue, especially the search-and-rescue (SAR) in post-disaster [1–6]. In this special case, most weak human victims trapped in collapsed buildings get injured seriously. Thus SAR crews must care about not only whether the victim is alive and where the victims is, but also what is the physiological status of the victims, which will be helpful for SAR crews to rescue the victims timely and efficiently. However, how to monitor the physiological parameters such as respiratory and heart rates

Received 30 September 2012, Accepted 5 November 2012, Scheduled 7 November 2012

* Corresponding author: Jian Qi Wang (wangjianqi@yahoo.com.cn).

† The first three authors contributed equally to this work and should be regarded as co-first authors.

with penetrating the debris is neglected in the practical application. Furthermore, it has been used to determine if human victims are still alive in situations where it may be dangerous to try to retrieve victims [7].

Current research on respiration and heartbeat monitoring mainly relies on the microwave impulse radar and continuous wave (CW) radar [7, 8], which can be widely used in monitoring health status of the patients in clinic or the old at home. However, these two types of radar are difficult to be applied in the non-line-of-sight (NLOS) scenes due to the poor penetrability. To improve the penetrability of nonmetallic obstacle, ultra-wideband (UWB) radar has been employed to detect vital sign of the victims in the NLOS scenes [9–16]. In these scenes, it mainly focuses on whether the victim is alive [16–23], namely life detection. It is realized based on accumulation of energy in a period of time, and signal-to-noise ratio (SNR) of vital sign can be improved. But it is very difficult to monitor the vital sign through the nonmetallic obstacle, especially the monitoring of heartbeat signal with extremely low SNR. To help rescue workers make optimal SAR measures in the post-disaster rescue, it is necessary to obtain the physiological parameters of human victims. Due to the interferences of clutter and noise, high signal attenuation of the obstacle, the realization of physiological parameters monitoring is challenging [2, 18]. Furthermore, the UWB radar should meet the need of both good penetrating ability and range resolution. This tradeoff makes this goal more challenging [11, 19].

Many research groups have tried to do some researches on this problem. Both respiration and heartbeat signals were obtained by the means of two different band-pass filters according to the frequency range [1]. Minimum Euclidian distance method in frequency domain was proposed to detect heartbeat parameter based on localization of the target and effective window size [24]. In [25], the respiration and heartbeat can be separated and detected by the wavelet based method, but the accurate selection of mother wavelet and its complexity limit the performance and application. Linear or parabolic approximated function was put forward to separate respiration and heartbeat based on threshold of the correlation of the function [26]. However, the performance is strongly dependent on the selection of approximated function. In this research as well as [27], Respiration and heartbeat can be obtained by the above methods only in the line-of-sight (LOS) scenes.

In some NLOS scenes, only respiration can be detected in [18, 19]. Both respiration and heartbeat were obtained with impulse radio (IR)-UWB radar proposed in [2]. Comb filter was used for respiratory

harmonics attenuation (HA) based on the detected fundamental frequency of respiration. This is because the level of the respiratory harmonics can be equal or even higher than the heartbeat signal with its low amplitude. In [28], Hilbert-Huang transform (HHT) was used to detect respiration and heartbeat of the human target behind the wall. However, the selection of intrinsic mode function (IMF) is empirical due to the overlap of frequency band. Moreover, this research [2, 18, 28] discussed above takes advantage of the UWB radar with high centre frequency (more than 1 GHz), which provides high spatial resolution but poor penetrability. The drawback limits its practical applications to some extent.

The aim of this paper is to propose a new method based on developed adaptive line enhancer (DALE) to monitor respiration and heartbeat of human target from UWB echo in NLOS scene. The quasi-periodic respiratory signal can be obtained adaptively by DALE due to time-variant parameters time delay and step-size, which is controlled by normalized least mean square (NLMS) algorithm. After respiration separation, the heartbeat signal is extracted from residual signal with moving target indicator (MTI) recursive filter and high order cumulant (HOC). The results of experiment show that this new method can be employed to monitor vital sign of human target through obstacle even with different body positions.

The remainder of this paper is organized as follows: UWB radar system is described in Section 2. This new method for vital sign monitoring is proposed in Section 3. Section 4 presents two data sets acquisition and the processed results of different experiments. Different motion responses due to respiration and heartbeat are discussed in Section 5. Lastly, concluding remarks of this paper are given in Section 6.

2. UWB RADAR SYSTEM DESCRIPTION

In our IR-UWB radar system, two polarized bow-tie antennas are used for transmission and reception, respectively. The Gaussian pulse is generated with an average transmit power of 5 mW and a pulse repetition frequency (PRF) of 250 kHz. The centre frequency of transmitted pulse is set as 400 MHz with the bandwidth of 200 MHz and pulse length of 5 ns. It complies with definition of UWB according to federal communication commission (FCC) regulation [29]. The reflected pulse is detected by the receiver and sampled by means of equivalent-time-sampling with different time delay. Thus we can obtain signals at these time delay, namely different ranges away from the radar. These signals from different ranges compose a received

waveform with range gating, amplification and integration. The block diagram of this IR-UWB radar system is shown in Figure 1(a). Due to the attenuation of free space with long distance or thick nonmetallic medium such as building ruins, weak vital sign is hard to be detected in these special cases. Thus, in order to compensate the attenuation, nonlinear amplification is used in our UWB system. The time-axis along the waveform associated to range (τ) is termed as "fast-time". Each received waveform along the range comprises 4096 points with time window of 40 ns. The sampling rate F_s of the radar system is 61.035 Hz, which means that the interval between successive received waveform is $T_s = \frac{1}{F_s} \approx 0.016$ s. The time-axis along this interval (t) is termed as "slow-time". Since the upper limit for the frequency of vital sign is about 3 Hz, the sampling rate is sufficient to capture both the respiratory motion and heartbeat motion according to the Nyquist sampling rate.

After sampling both in fast time $\tau = mT_f$ $(m = 1, 2, \ldots, M)$ and slow time $t = nT_s$ $(n = 1, 2, \ldots, N)$, N received waveforms are stored in the data matrix R, which can be written as $R[m, n] = r$ $(\tau = mT_f,\ t = nT_s)$. Each column of this matrix contains one received waveform. A received waveform and its spectrum are shown in Figures 1(b) and (c), respectively.

3. METHOD FOR VITAL SIGN MONITORING

In the vital sign detection with IR-UWB radar system, the received signal can be written as the sum of convolution of transmit pulse and channel impulse response [2]. The result can be written as:

$$r(\tau, t) = \sum_i A_i p(\tau - \tau_i) + Bp(\tau - \tau_d(t)) + \theta(t) \tag{1}$$

where $\sum_i A_i p(\tau - \tau_i)$ corresponds to the reflection of static background, $Bp(\tau - \tau_d(t))$ corresponds to the reflection of human target, and $\theta(t)$ is unwanted additive noise. $\tau_d(t)$ is time delay related to the periodical motion of chest cavity. Traditionally, this periodical motion is expressed as sum of two different sinusoids associated to the respiration and heartbeat of the stationary human target

$$\tau_d(t) = 2d(t)/c = 2\frac{d_0}{c} + \frac{2A_r}{c}\sin(2\pi f_r t) + \frac{2A_h}{c}\sin(2\pi f_h t) \tag{2}$$

where f_r and f_h denote respiratory frequency and heartbeat frequency, respectively. A_r and A_h are the displacement amplitudes of respiration and heartbeat. d_0 is the distance between the chest movement center and radar and c the light speed in the air. From (1) and (2), vital sign

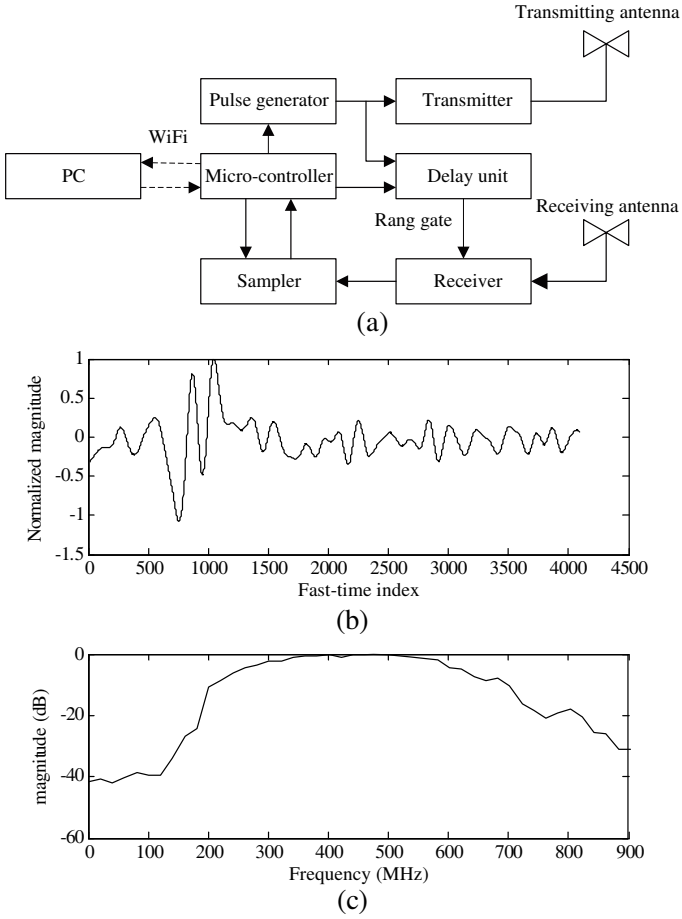

Figure 1. (a) The block diagram of the IR-UWB radar system. (b) One received waveform. (c) The spectrum of the received waveform.

of the human target should be contained in some rows of data matrix R. These rows are called target rows in this paper.

The new method is proposed to extract and monitor vital sign mixed with static background and additive noise. Each implementation of this method is shown in Figure 2. It consists of four main parts. First, raw echo is preprocessed to improve the SNR of vital sign. Then, DALE is used to separate and extract respiration. After that, respiratory harmonics are attenuated by MTI excursive filter. At last, HOC is implemented to improve and extract heartbeat.

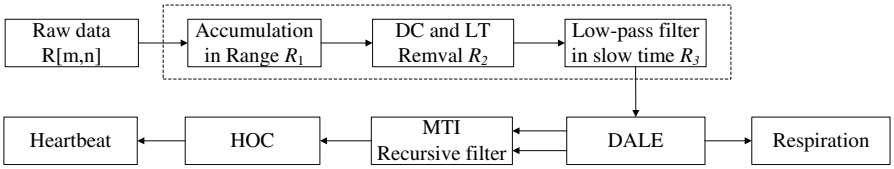

Figure 2. The flowchart of signal processing.

3.1. Signal Preprocessing

Three steps of signal preprocessing are shown in the dotted box in Figure 2. The useful signals coming from neighboring target rows in the row data are modulated by the respiratory and heartbeat movement of human target [19]. Therefore, range average in the fast-time increases the SNR of received signal. This step can be written as

$$R_1[x,n] = \frac{1}{Q} \sum_{m=(x-1/2\,)Q}^{(x+1/2\,)Q-1} R[m,n] \tag{3}$$

where $x = 1, 2, \ldots, X$, Q is the window size in the fast-time dimension, and $X = \lfloor \frac{M}{Q} \rfloor$ is the compression result in the same dimension. $\lfloor a \rfloor$ denotes the largest integer less than a.

Vital sign is totally buried in the strong static background [2]. Traditionally, motion filter is used to suppress the reflection of static background manifested as a DC component. However, the instability of radar can lead to a linear trend (LT) or amplitude instability in the slow-time dimension [18]. So linear trend subtraction (LTS) method is employed to remove DC component and LT

$$R_2^T = R_1^T - \mathbf{Y}\left(\mathbf{Y}^T\mathbf{Y}\right)^{-1}\mathbf{Y}^T R_1^T \tag{4}$$

where $\mathbf{Y} = [\mathbf{n}/N, \mathbf{1}]$ is a $N \times 2$ matrix, $\mathbf{n} = [0, \ldots, , N-1]$, N the number of stored waveform in matrix R_1, and $\mathbf{1}$ a vector of ones of length N.

In low-pass filter, the cutoff frequency is set according to the frequency range of vital sign so as to remove some high frequency components of the received signal. The result of this step is denoted by R_3.

3.2. Developed Adaptive Line Enhancer

As an especial degenerate form of adaptive noise cancellation, adaptive line enhancer (ALE) doesn't need a separate reference signal, which can be obtained by a constant delay version of the input signal [30]. In

ALE, reference signal $d(n)$ is processed by a FIR transversal filter to generate an error signal $e(n)$, expressed as the difference between input signal and ALE's output $y(n)$. Moreover, the error signal $e(n)$ is used to actuate the convergence algorithm for adjusting weight vector $\mathbf{W}(n)$ of FIR filter so as to minimize the value of $e(n)$. Conventionally, ALE is used to detect a narrowband sinusoidal signal buried in a wideband noise background based on the fact that optimal delay version can remove the correlation of noise between input and reference signal. In order to separate and extract the nonstationary and quasi-periodic respiration from echo, a DALE is proposed based on the same theory of ALE, but with adaptive adjusting time delay and NLMS convergence algorithm.

The schematic diagram of this developed filter is presented in Figure 3. Each row of preprocessed data matrix R_3 will be used as input of DALE. When target row $r_3(n)$ is input into DALE, it can be written as

$$r_3(n) = s_r(n) + s_h(n) + \eta(n) \tag{5}$$

where s_r and s_h denote respiratory signal and heartbeat signal, respectively. $\eta(n)$ is residual noise of $\theta(n)$. The reference signal is generated by the time-varying delayed version Z_n in sample. This parameter is determined by bandwidths of respiration and heartbeat

$$P_h < Z_n/Fs < P_r \tag{6}$$

where P_h and P_r are the periods of heartbeat and respiration. Z_n/F_s denotes the delay version in time. It is assigned a value large enough to remove the correlations of heartbeat signal and broadband noise between input and reference signal, respectively, whereas only respiration in input and reference signal is correlated. Thus the cross correlation between $r_3(n)$ and $d(n)$ is given by

$$\hat{R}_{dr_3}(k) = E[r_3(n)r_3(n - Z_n - k)] = E[s_r(n)s_r(n - Z_n - k)]. \tag{7}$$

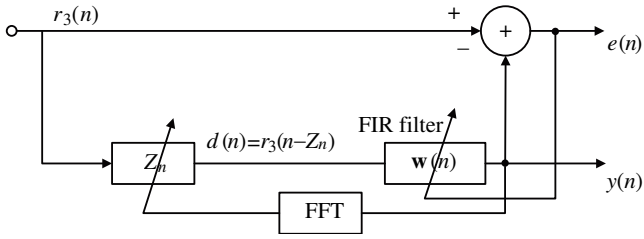

Figure 3. The schematic diagram of DALE.

When the DALE FIR filter has converged to its Wiener filter coefficients, the output of FIR and error signal can be estimated by

$$y(n) = \mathbf{w}^T(n)\mathbf{d}(n) \approx s_r(n) \tag{8}$$

$$e(n) = r_3(n) - y(n) \approx s_h(n) + \eta(n), \tag{9}$$

respectively. The output $y(n)$ is in response to a reference signal vector $\mathbf{d}(n)$ based on current estimate of the tap-weight vector $\mathbf{w}(n)$, and error signal is used for heartbeat extraction. However, output $y(n)$ will be distorted even diffusive, when the large magnitude instability of received signal occurs. This is because the received signal of radar and respiration are conventionally nonstationary. To handle the nonstationary input, and thus a nonstationary reference signal, the NLMS algorithm is proposed to adjust current estimate of the tap-weight vector, which can be written as

$$\mathbf{W}(n+1) = \mathbf{W}(n) + \frac{\mu_0}{\xi + \|\mathbf{d}(n)\|^2} e(n)\mathbf{d}(n) \tag{10}$$

where positive real scaling factor μ_0 and small positive real number ξ are in the range $(0, 1)$ in this paper. If the denominator $\mathbf{d}(n)$ is too large or small, the convergence rate can't change extremely with the help of these two parameters. Thus the convergence rate can be adjusted by the power of nonstationary reference vector $\mathbf{d}(n)$ automatically, and convergence of DALE with NLMS is potentially faster and safer than that of standard least-mean-square (LMS) algorithm.

In this paper, adjustable parameter Z_n is mainly dependent on respiration rate because the frequency ranges of respiration and heartbeat are quite different and the heartbeat is relatively stable in the normal situation. Therefore, delay version Z_n can be adjusted automatically according to the change of respiration rate estimated by the FFT result of $y(n)$ after some iteration. This result will also be used to trace the change of respiration in HA.

In this subsection, respiration and heartbeat can be separated adaptively by DLAE instead of band-pass filter with high performance. Conventionally, due to the instability of the vital sign, the design and realization of the latter is not easy. Furthermore, when the input of DALE is not the target row, there are only noise and interference in the input. According to the theory of ALE, the FIR filter is locked in this situation. Hence, DALE changes into an all-pass filter theoretically, and the error signal approximates input.

3.3. Respiratory Harmonics Attenuation

In the UWB echo, the heartbeat signal is so weak that it is easy to be covered by the strong nonstationary respiratory harmonics [2, 27].

Thus these harmonics should be suppressed accurately. MTI recursive filter is proposed to attenuate respiratory harmonics adaptively based on time-variant time delay. This parameter is determined by the change of respiration, which can be obtained from DALE. The structure of MTI recursive filter is shown in Figure 4.

Power gain of this filter in frequency domain is given by

$$|H(\omega)|^2 = \frac{2(1-\cos\omega P_r)}{(1+K)^2 - 2K(\cos\omega P_r)} \tag{11}$$

where $\omega = 2\pi f$ and P_r is the respiration period estimated by DALE. Equation (11) shows the amplitude response is periodic with a period equal to $1/P_r$, and nulls occur at $f \cdot P_r = i$, $i = 0, 1, 2 \ldots$. Therefore, this filter can suppress the respiratory harmonics effectively, as well as the residual DC component. Figure 5 shows the power gain of MTI recursive filter as a function of normalized frequency f/f_r. As increasing the value of K, the stop-band narrows down. Thus only respiratory harmonics instead of heartbeat component are attenuated in HA, when the frequency of heartbeat is not a multiple of the fundamental frequency of respiration.

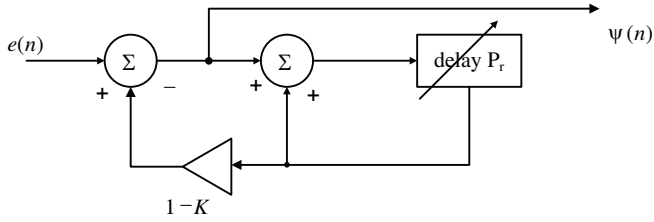

Figure 4. The schematic diagram of MTI recursive filter.

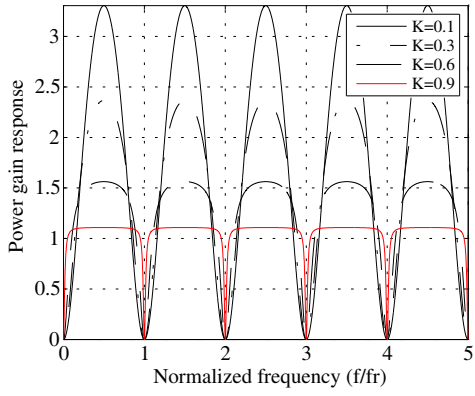

Figure 5. The power gain of MTI recursive filter as a function of normalized frequency for $K = 0.1, 0.3, 0.6, 0.9$.

3.4. High Order Cumulant

HOC method is provided to improve and extract heartbeat signal in this subsection. This is because HOC of any color Gaussian noise is zero theoretically, and this method is insensitive to stochastic noise and interference. According to the definition of HOC [31], the fourth-order cumulant of $\psi(n)$ can be written as

$$C_{4\psi}(\upsilon_1,\upsilon_2,\upsilon_3)=C_{4s_h}(\upsilon_1,\upsilon_2,\upsilon_3)+C_{4\eta}(\upsilon_1,\upsilon_2,\upsilon_3)=C_{4s_h}(\upsilon_1,\upsilon_2,\upsilon_3) \quad (12)$$

where cumulant of noise $C_{4\eta}(\upsilon_1,\upsilon_2,\upsilon_3)=0$. The Equation (12) can be calculated as

$$\begin{aligned} C_{4s_h}(\upsilon_1,\upsilon_2,\upsilon_3) = {} & \hat{m}_{4s_h}(\upsilon_1,\upsilon_2,\upsilon_3) - \hat{R}_{s_h}(\upsilon_1)\hat{R}_{s_h}(\upsilon_3-\upsilon_2) \\ & -\hat{R}_{s_h}(\upsilon_2)\hat{R}_{s_h}(\upsilon_3-\upsilon_1)-\hat{R}_{s_h}(\upsilon_3)\hat{R}_{s_h}(\upsilon_2-\upsilon_1) \end{aligned} \quad (13)$$

where $\hat{m}_{4s_h}$ and $\hat{R}_{s_h}$ are fourth-order moment and correlation of heartbeat signal s_h, respectively. So HOC of s_h can be expressed as

$$\begin{aligned} C_{4s_h}(\upsilon,\upsilon,\upsilon) = {} & \frac{1}{N}\sum_{n=1}^{N}\left(s_h(n){s_h}^3(n+\upsilon)\right) \\ & -\frac{3}{N^2}\sum_{n=1}^{N}\left(s_h(n)s_h(n+\upsilon)\right)\sum_{n=1}^{N}{s_h}^2(n). \end{aligned} \quad (14)$$

where $\upsilon_1=\upsilon_2=\upsilon_3=\upsilon$. According to (2), heartbeat signal is regarded as a sinusoid. Thus 1-D slice of fourth-order cumulant of heartbeat is written as

$$C_{4s_h}(\upsilon)=-\frac{3}{8}\left(\sum_{i=1}^{\infty}A_{hi}^4\cos i\omega_h\upsilon\right) \quad (15)$$

where $\omega_h=2\pi f_h$, and A_{hi} is related to the magnitude of heartbeat.

After DALE, the target row which contains strongest energy of respiration can be obtained with the method of maximum variance proposed in [11]. Thus, the human target can be localized, and this target row is used to extract heartbeat signal directly. Therefore, the respiration and heartbeat monitoring of human target can be realized.

4. EXPERIMENTS AND RESULTS

In this section, two types of experimental data are acquired to verify the capability of vital sign monitoring in the real scenarios with this new method. The scenarios of the measurement are shown in Figure 6. Both experiments were carried out in our lab, and thickness of brick wall is 28 cm. By the way, the parameters of radar system were described in Section 2.

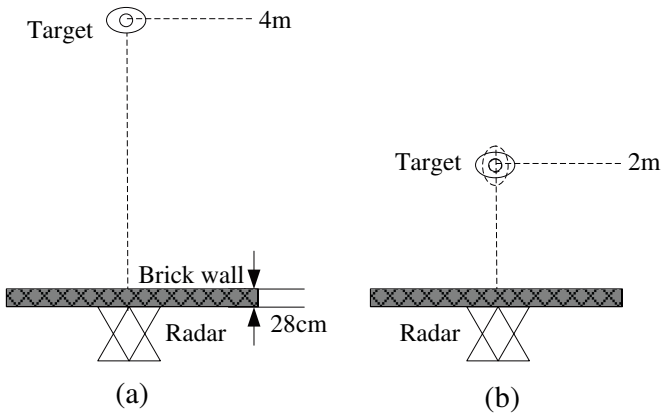

Figure 6. Experiments performed behind the wall. (a) Human target is located 4 m away from radar. (b) Human target is located 2 m away from radar but with different positions.

4.1. Experimental Scenarios

In the first case, one stationary human target with normal breath headed directly toward the radar as shown in Figure 6(a). The distance between human target and IR-UWB radar is 4 m. While, in the second case, the distance between radar and the same human target is 2 m. In this case, in order to simulate trapped positions of survivors under the building ruins, the human target stands behind the standard brick wall with three positions of face to face, face to back and face to side, respectively. First position has been presented in the former experimental scenario. Human target faces opposite direction in the second position where the human back faces the radar straightly. In the last position, human target rotates 90° from the first position with the arm towards to the radar.

4.2. Results

Respiratory and heartbeat results of two experiments are shown in this subsection, respectively. Moreover, the performances of this proposed method and other methods are compared.

Figure 7 shows the received and processed data matrix of the first experiment as a function of range and slow-time indexes. Received raw data is shown in Figure 7(a) where the vital sign is totally submerged in static background. The output of DALE FIR filter is shown in Figure 7(b). This figure clearly shows the signal fluctuation

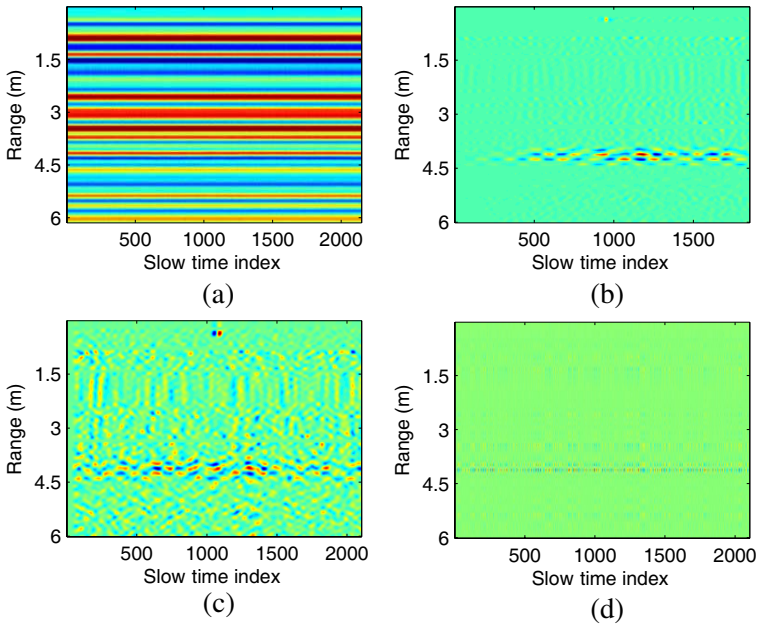

Figure 7. (a) Raw data matrix without any signal processing. (b) Result data matrix after implementation of DALE with preprocessed data. (c) Result data matrix after implementation of band-pass filter with preprocessed data. (d) Result data matrix after implementation of SVD with preprocessed data.

due to the small respiratory movement. In order to compare the performances of this new method and other methods, conventional band-pass filter and SVD method proposed in [18] are chosen for the comparison. Figures 7(c) and (d) show the results of data matrix processed by these two methods, respectively. It is obviously that our new method has better performance in the respiration extraction. In Figure 7(c), though the vital sign is visible, it is contaminated seriously by some interference of nonstationary clutter and noise. The respiration monitoring must be disturbed, and extracted respiratory signal is distorted. The result of SVD shown in Figure 7(d) is better than that in Figure 7(c), but the respiration is much weaker comparing with Figure 7(b). We can find some clutters still exist in Figure 7(d). Furthermore, the decision space of SVD that contains respiration must be derived properly and empirically. The rank of decision space equals two in this experiment, but not equals one as discussed in [18].

Figure 8 shows the results of respiration and heartbeat monitoring

in the first experiment after signal processing of our new method. Respiratory slow-time signal of human target is shown in Figure 8(a), and the instability of respiration can be seen in this figure. Figure 8(b) shows the Fourier transform of this signal, in which the frequency of respiration is clearly estimated at 0.272 Hz by finding the maximum peak. The extracted heartbeat signal in slow-time is shown in Figure 8(c), and its frequency can be estimated at 1.313 Hz from its spectral result shown in Figure 8(d).

The data matrices processed by DALE in the second experiment are shown in Figure 9, respectively. Respirations of three positions are all clearly detected and shown in this figure, but the respiratory-motion responses are different. Figure 9(a) shows that face to face position has the best respiratory-motion response, while Figure 9(c) shows that respiratory-motion response of face to side position is much weaker than that of the other two positions. Moreover, some nonstationary clutters obviously exist at the further range in Figure 9(c). This

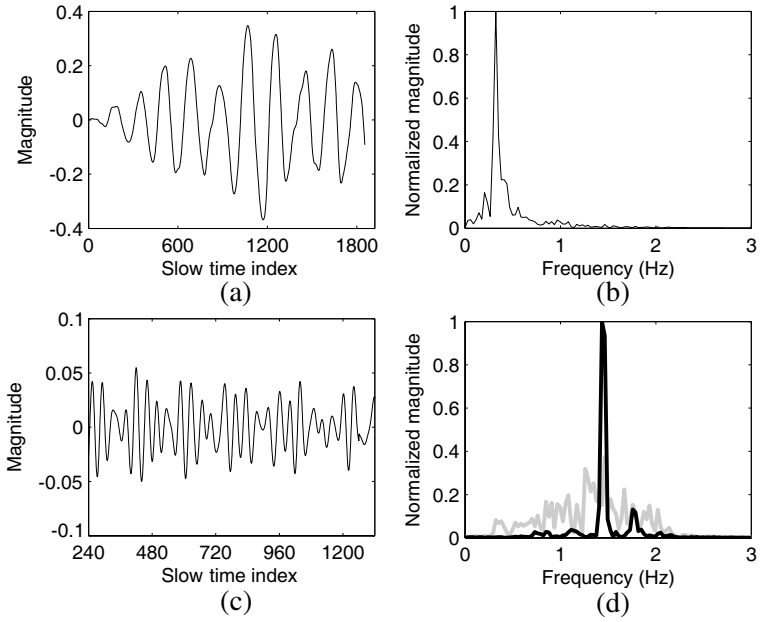

Figure 8. Vital sign of human target located 4 m away from radar. (a) Respiratory signal in slow-time dimension. (b) Spectral result of respiratory signal. (c) One segment of heartbeat signal in slow-time dimension. (d) Spectral results of heartbeat signal before and after signal processing of HA and HOC.

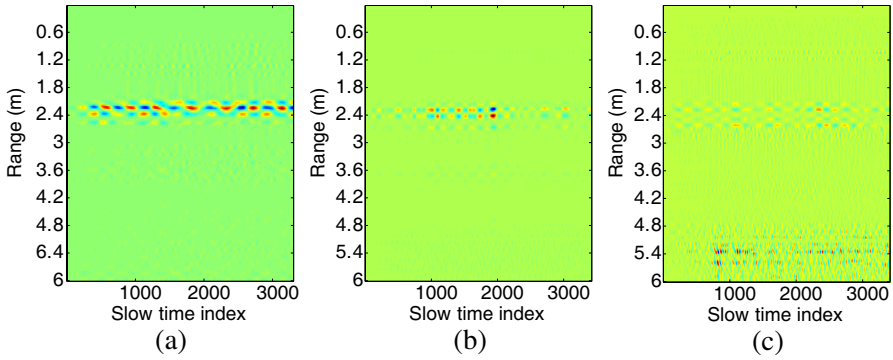

Figure 9. (a) Respiratory-motion response of face to face position. (b) Respiratory-motion response of face to back position. (c) Respiratory motion response of face to side position.

nonstationary clutter is bad for vital sign monitoring. In this figure, range of respiratory-motion response is wider along the fast-time dimension. Therefore, the face to face position of human target is best for the human target detection and respiration monitoring.

In Figure 9, range locations of human target l_r are all about 2.4 m. This is because the path of electromagnetic wave of UWB radar in the brick wall corresponding to that in the air changes longer [19, 27]. However, these results can be modified by the formula

$$l_t = l_r - d(\sqrt{\varepsilon_r} - 1) \tag{16}$$

where $d = 0.28$ m is the thickness of the brick wall. The measured average dielectric constant of the rubble ε_r equals 4.5. Thus, real range location l_t of face to face position is calculated at the distance of 2.03 m from the radar to the target. In the other two positions, real range locations are 2.07 m and 1.96 m in the face to back position and face to side position, respectively. Human target in the last position is the nearest to the radar.

Figure 10 shows the results of extracted respiration in three different positions, respectively. In this figure, the magnitudes of different respiratory signals in slow-time just coincide with the corresponding respiratory-motion response shown in Figure 9. In Figure 10(a), face to face position has the largest magnitude of respiratory signal. Figure 10(b) shows the normalized spectral results of respiratory signals. In this figure, it is obviously that the respiratory slow-time signal in face to back position has some low-frequency components, and SNR of respiratory signal in face to side position is the lowest [27]. The frequencies of respiration in different positions are estimated at 0.278 Hz, 0.264 Hz and 0.249 Hz, respectively.

The normalized spectral results of heartbeat signals before and after signal processing of HA and HOC are shown in Figure 11. Though the heartbeat signals are much weaker than respiratory signals, features of heartbeat-motion response shown in Figure 11(b) are similar to that of respiratory-motion response. Face to face position still has the strongest heartbeat-motion response whereas face to side position has the weakest one. Heartbeat frequencies are estimated at 1.289 Hz, 1.304 Hz and 1.318 Hz in these three positions, respectively.

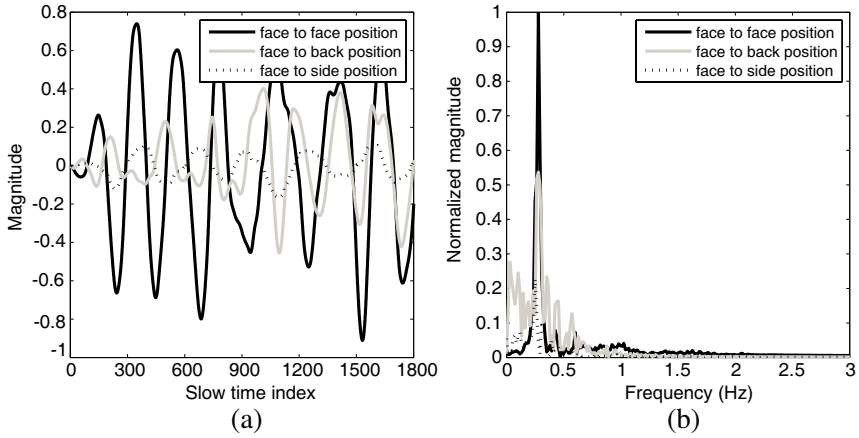

Figure 10. (a) Respiratory slow-time signals at modified range of different positions. (b) Normalized spectral results of respiratory signals in frequency domain.

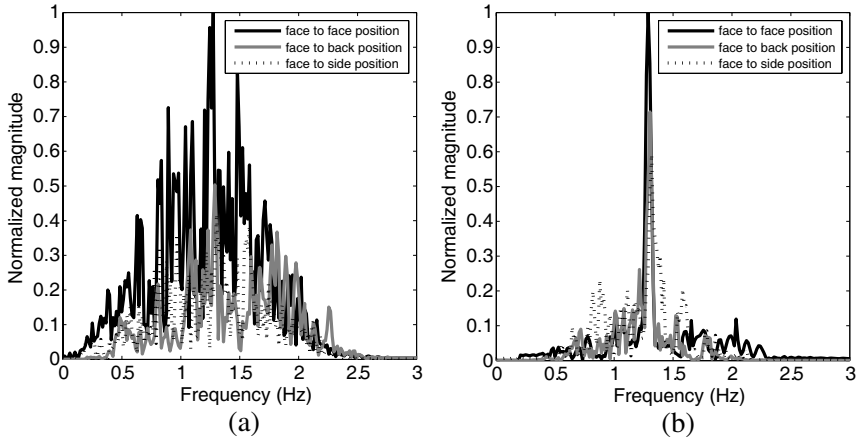

Figure 11. The spectral results of heartbeat signals in the second experiment. (a) Before and (b) after signal processing of HA and HOC.

5. DISCUSSION

In this section, the performance of combination of HA and HOC is studied quantitatively. In addition, motion responses resulted from respiration and heartbeat in the UWB echo are also discussed.

In Figure 8(d) and Figure 11, the spectral results show that the heartbeat signal is improved obviously after signal processing of HA and HOC. For the quantitative analysis, the SNR of heartbeat signal is redefined in the frequency domain

$$SNR_{f_h} = 20\log_{10}\left(\frac{|F(f_h)|}{\frac{1}{L}\sum\limits_{f=0,f\neq f_h}^{F_H}|F(f)|}\right) \tag{17}$$

where $|F(\cdot)|$ denotes the magnitude of spectral result, $F_H = 3\,\text{Hz}$ the upper limit of heartbeat frequency, f_h the heartbeat frequency, and L the number of frequency values in the frequency range except heartbeat frequency. $|F(f_h)|$ and $\frac{1}{L}\sum\limits_{f=0,f\neq f_h}^{F_H}|F(f)|$ are regarded as the energy of the heartbeat and noise, respectively. Calculations of SNR are shown in Table 1. In this table, the results show that SNR of heartbeat signal can be improved effectively by the combined method of HA and HOC. The SNR of face to face position is the largest whereas face to side position has the lowest SNR. The maximum improvement of SNR is about 20 dB.

All the respiratory-motion responses of three positions are shown in Figure 9. In this figure, face to face position has the best respiratory-motion response, and respiratory-motion response of the face to side position is much weaker than that of the other two positions. This is because the face to side position has the smallest effective radar cross section (ERCS) of respiration [32]. By comparing Figures 9(a) and (b), the respiratory-motion response of face to back position is still weaker

Table 1. SNR of heartbeat signals in different experiments.

	Experiment 1	Face to face[a]	Face to back[a]	Face to side[a]
$SNR^b_{f_h}$	15.379 dB	15.573 dB	14.831 dB	13.901 dB
$SNR^c_{f_h}$	33.140 dB	35.296 dB	26.973 dB	21.871 dB

[a] denotes position in the second experiment.
[b] and [c] denote signal processing before and after HA and HOC.

than that of face to face position. Different detected displacement magnitude of chest cavity in these two positions may be the reason for this phenomenon [32]. Moreover, Figure 9(c) shows that range of respiratory-motion response along the fast-time is wider than that of other two positions. This is caused by the width of human body in the face to side position. Thus this wide respiratory-motion response and interference of nonstationary clutter make vital sign monitoring more challenging. For the heartbeat-motion response, face to face position is still the strongest whereas face to side position has the weakest response. This can be explained by the fact that the motion of the heart translated to the front is much stronger than that to the back. This result also coincides with analysis of cardiopulmonary ERCS in the vital sign monitoring with Doppler radar system [32].

6. CONCLUSION

Previous researches of NLOS vital sign detection mainly aim at life detection based on respiration detection and extraction. In this paper, we have proposed a novel method based on DALE to monitor both respiration and heartbeat in NLOS scenes. Two cases of experiments have been conducted to study the performance of this new method. Especially, in the second case, possible positions of trapped victim under the building ruins are simulated by three different positions. When the human target is located 2 m away from UWB radar, both respiration and heartbeat can be obtained in all three positions. Furthermore, the motion responses due to respiration and heartbeat are compared and discussed in this paper. Face to face position is the best suitable position for the human detection and monitoring. This is meaningful for the SAR crews to detect trapped survivors and obtain their accurate physiological parameters in post-disaster rescue.

In our future work, the nonstationary clutter removal should be taken into account in more complex scenarios such as simulated rubbles even the real post-earthquake building ruins.

ACKNOWLEDGMENT

This work was supported by the National Natural Science Foundation of China (Grant Nos. 60927003 and 60801059) and National Science & Technology Pillar Program (Grant No. 2012BAI20B02). The authors would like to thank M. Liu and Q. An for their valuable assistance on data acquisition.

REFERENCES

1. Immoree, I. and T.-H. Tao, "UWB radar for patient monitoring," *IEEE Aerospace and Electronic Systems Magazine*, Vol. 23, No. 11, 11–18, 2008.
2. Lazaro, A., D. Girbau, and D. Villarino, "Analysis of vital signs monitoring using an IR-UWB radar," *Progress In Electromagnetics Research*, Vol. 100, 265–284, 2010.
3. Ramos, A., A. Lazaro, D. Girbau, and R. Villarino, "Time-domain measurement of time-coded UWB chipless RFID tags," *Progress In Electromagnetics Research*, Vol. 116, 221–237, 2011.
4. Zhang, Z. and Y. Lee, "A robust cad tool for integrated design of UWB antenna system," *Progress In Electromagnetics Research*, Vol. 112, 441–457, 2011.
5. Alshehri, S. A., S. Khatun, A. B. Jantan, R. S. A. Raja Abdullah, R. Mahmood, and Z. Awang, "Experimental breast tumor detection using nn-based UWB imaging," *Progress In Electromagnetics Research*, Vol. 111, 447–465, 2011.
6. Alshehri, S. A., S. Khatun, A. B. Jantan, R. S. A. Raja Abdullah, R. Mahmood, and Z. Awang, "3D experimental detection and discrimination of malignant and benign breast tumor using nn-based UWB imaging system," *Progress In Electromagnetics Research*, Vol. 116, 221–237, 2011.
7. Mikhelson, I. V., S. Bakhtiari, T. W. Elmer, and A. V. Sahakian, "Remote sensing of heart rate and patterns of respiration on a stationary subject using 94-GHz millimeter-wave interferometry," *IEEE Trans. Biomed. Eng.*, Vol. 58, No. 6, 1671–1677, 2011.
8. Yang, Y., S. M. Royg, N. C. Karmakar, and X. Zhu, "A novel narrow bandpass filter for image rejection and channel selection in a wireless sleep apnoea monitoring system," *Progress In Electromagnetics Research*, Vol. 125, 483–501, 2012.
9. Zhang, W., A. Hoorfar, and L. Li, "Through-the-wall target localization with time reversal music method," *Progress In Electromagnetics Research*, Vol. 106, 75–89, 2010.
10. Jia, Y., L. Kong, and X. Yang, "A novel approach to target localization through unknown walls for through-the-wall radar imaging," *Progress In Electromagnetics Research*, Vol. 119, 107–132, 2011.
11. Li, Y., X. Jing, H. Lv, and J. Wang, "Analysis of characteristics of two close stationary human targets detected by impulse radio UWB radar," *Progress In Electromagnetics Research*, Vol. 126, 429–447, 2012.

12. McGinley, B., M. O'Halloran, R. C. Conceicao, G. Higgins, E. Jones, and M. Glavin, "The effects of compression on ultra wideband radar signals," *Progress In Electromagnetics Research*, Vol. 117, 51–65, 2011.
13. Shaban, H. A., M. A. El-Nasr, and R. M. Buehrer, "Localization with sub-millimeter accuracy for UWB-based wearable human movement radar systems," *Journal of Electromagnetic Waves and Applications*, Vol. 25, Nos. 11–12, 1633–1644, 2011.
14. Wong, S. K., F. Kung, S. Maisurah, and M. N. B. Osman, "A wimedia compliant cmos RF power amplifier for ultra-wideband (UWB) transmitter," *Progress In Electromagnetics Research*, Vol. 112, 329–347, 2011.
15. Lizzi, L., G. Oliveri, and A. Massa, "A time-domain approach to the synthesis of UWB antenna systems," *Progress In Electromagnetics Research*, Vol. 122, 557–575, 2012.
16. Zhu, F., S. Gao, A. T. S. Ho, C. H. See, R. A. Abd-Alhameed, J. Li, and J. Xu, "Design and analysis of planar ultra-wideband antenna with dual band-notched function," *Progress In Electromagnetics Research*, Vol. 125, 483–501, 2012.
17. Andres-Garcia, B., L. E. Garcia-Munoz, D. Segovia-Vargas, I. Camara-Mayorga, and R. Gusten, "Ultrawideband antenna excited by a photomixer for terahertz band," *Progress In Electromagnetics Research*, Vol. 114, 1–15, 2011.
18. Nezirovic, A., A. G. Yarovoy, and L. P. Ligthart, "Signal processing for improved detection of trapped victims using UWB radar," *IEEE Trans. Geosci. Remote Sens.*, Vol. 48, No. 4, 2005–2014, 2010.
19. Lv, H., G. H. Lu, X. J. Jing, and J. Q. Wang, "A new ultra-wideband radar for detecting survivors buried under earthquake rubbles," *Microwave Opt. Technol. Lett.*, Vol. 52, No. 11, 2621–2624, 2010.
20. Zhu, F., S. C. S. Gao, A. T. S. Ho, T. W. C. Brown, J. Li, and J. D. Xu, "Low-profile directional ultra-wideband antenna for see-through-wall imaging applications," *Progress In Electromagnetics Research*, Vol. 121, 121–139, 2011.
21. Crowgey, B. R., E. J. Rothwell, L. C. Kempel, and E. L. Mokole, "Comparison of UWB short-pulse and stepped-frequency radar systems for imaging through barriers," *Progress In Electromagnetics Research*, Vol. 110, 403–419, 2010.
22. Tian, B., D. Y. Zhu, and Z. D. Zhu, "A novel moving target detection approach for dual-channel SAR system," *Progress In Electromagnetics Research*, Vol. 115, 191–206, 2011.

23. Li, B., Z. Zhou, D. Li, and S. Zhai, "Efficient cluster identification for measured ultra-wideband channel impulse response in vehicle cabin," *Progress In Electromagnetics Research*, Vol. 117, 121–147, 2011.
24. Baboli, M., A. Sharafi, A. Ahmadian, and M. S. Nambakhsh, "An accurate and robust algorithm for detection of heart and respiration rates using an impulse based UWB signal," *International Conference on Biomedical and Pharmaceutical Engineering, ICBPE'09*, 13–18, 2009.
25. Ossberger, G., T. Buchegger, E. Schimback, A. Stelzer, and R. Weigel, "Non-invasive respiratory movement detection and monitoring of hidden humans using ultra wideband pulse radar," *Proc. of the 2004 International Workshop on Ultra Wideband Systems Joint with Conference on Ultra Wideband Systems and Technologies*, 395–399, Piscataway, NJ, USA, 2004.
26. Pavlov, S. and S. Samkov, "Algorithm of signal processing in ultra-wideband radar designed for remote measuring parameters of patient's cardiac activity," *Ultrawideband and Ultrashort Impulse Signals, 2004 Second International Workshop*, 204–207, 2004.
27. Xu, Y., S. Dai, S. Wu, J. Chen, and G. Fang, "Vital sign detection method based on multiple higher order cumulant for ultrawideband radar," *IEEE Trans. Geosci. Remote Sens.*, Vol. 50, No. 4, 1254–1265, 2012.
28. Liu, Z., L. Liu, and B. Barrowes, "The application of the Hilbert-Huang transform in through-wall life detection with UWB impulse radar," *PIERS Online*, Vol. 6, No. 7, 695–699, 2010.
29. Federal Communications Commission (FCC), "First report and order in the matter of revision of Part 15 of the commission's rules regarding ultra-wideband transmission systems," ET Docket 98–153, FCC 02-48, Apr. 2002.
30. Li, W., X. Jing, Z. Li, and J. Wang, "A new algorithm for through wall human respiration monitoring using GPR," *14th International Conference on Ground Penetrating Radar (GPR)*, 947–952, 2012.
31. Mendel, J. M., "Tutorial on higher-order statistics (spectra) in signal processing and system theory: Theoretical results and some applications," *Proc. IEEE*, Vol. 79, No. 3, 278–305, 1991.
32. Kiriazi, J. E., O. Boric-Lubecke, and V. M. Lubecke, "Dual-frequency technique for assessment of cardiopulmonary effective RCS and displacement," *IEEE Sens. J.*, Vol. 12, No. 3, 574–582, 2012.